

LASER PLASMA

PACS numbers: 41.75.Fr; 52.38.Fz; 52.20.Fs
DOI: 10.1070/QE2006v036n08ABEH013281

Simulations of electron-beam scattering by spontaneous magnetic fields in a laser plasma

P.V. Konash, I.G. Lebo

***Abstract*. The feasibility of experimental investigation of spontaneous magnetic fields in a laser plasma with the help of a fast-electron beam is discussed. A three-dimensional program was written to calculate the kinetics of these electrons in sign-variable magnetic fields and calculations were made for different plasma parameters. An electron energy of ~100 keV is shown to be sufficient for the investigation of magnetic fields in the plasma plume; this energy for a compressed laser target ranges between 4 and 8 MeV. Electrons with this energy can be generated employing an additional picosecond laser pulse synchronised with the main heating pulse.**

Keywords: *magnetic fields in plasma, electron scattering, laser-produced plasma.*

1. Introduction

Spontaneous magnetic fields (SMFs) in a laser-induced spark [1] and in the laser irradiation of a condensed target [2] were first observed in the late 1960s. They were recorded by using wire probes placed in the vicinity of the plasma objects. Theoretical research performed in the 1970s showed that the fields generated inside the plasma may fall into the megagauss range [3 – 8]. The principal generation mechanism of these fields, at least for moderate intensities of laser radiation (i.e., for $q\lambda^2 < 10^{15}$ W cm^{-2} μm^2, where q is the intensity of laser radiation in W cm^{-2} and λ is the radiation wavelength in μm) is the thermal EMF in a nonuniform plasma: the emergence of noncollinear temperature and density gradients. For high intensities of laser radiation, other mechanisms may also be responsible for the generation of ultrahigh magnetic fields (see, for instance, Refs [9 – 10]).

To simulate these processes in plasmas, two-dimensional programs were developed in our country and abroad, which allow obtaining numerical solutions of the equations of magnetic gas dynamics [11 – 14]. Numerical solutions confirmed theoretical estimates and enabled studying the localisation of the fields in the plasma, their effect on dynamics and heat transfer.

P.V. Konash, I.G. Lebo Moscow State Institute of Radio Engineering, Electronics and Automatics (Technical University), prosp. Vernadskogo, 78, 119454 Moscow, Russia; e-mail: lebo@mirea.ru

Received 14 March 2006
Kvantovaya Elektronika **36** (8) 767 – 772 (2006)
Translated by E.N. Ragozin

Experimental techniques were also elaborated for SMF observation directly in the plasma, which were primarily based on the well-known Faraday effect: during the propagation of a plane-polarised laser beam along a magnetic line of force, the plane of polarisation rotates about the axis coincident with the direction of the magnetic line of force. By using these techniques, it was possible to observe the fields in expanding low-density laser-produced plasmas [15 – 18]. It was found that the SMFs generated in a compressed laser target may, owing to strong pressure and density gradients, be two orders of magnitude higher than in the plasma corona [19]. Unfortunately, traditional optical techniques do not enable looking into the depth of a compressed target. SMF research is topical, which is due to the fact that active work is presently underway to construct megajoule laser systems for initiating thermonuclear 'bursts'.

Along with applied problems, on these facilities it is planned to pursue investigations in astrophysical plasma modelling. Magnetic fields are known to play a significant role in stellar dynamics, and therefore observing such fields in compressed laser targets is of interest at the present time. The authors of Refs [19 – 22] discussed the feasibility of observing SMFs in compressed targets by two methods based on recording the escape anisotropy of charged thermonuclear particles (secondary protons and alpha particles) and electron beam scattering by the SMFs in the target. Unfortunately, the technical realisation of these ideas in the 1980s proved to be too complicated.

In connection with the investigations in separate compression and fast ignition of thermonuclear reactions [23 – 27], major facilities, in addition to a large number of 'long-pulse' (10 – 100 ns) laser beams, provision for the generation of short (1 – 10 ps) laser pulses, which in principle may be employed to generate high-energy laser beams. These beams can be synchronised with the main laser pulse.

In the present paper we do not discuss the mechanisms of the production and formation of the diagnostic electron beam. Below, we formulate the SMF diagnostics problem and briefly describe the methods of its solution; also given are the results of the numerical simulation of electron beam scattering by the SMFs in the laser plasma.

2. Physical formulation of the problem

It is evident that the proposed technique of SMF observation in a compressed laser target should be elaborated using simpler objects than a multibeam laser thermonuclear facility. We need only have at our disposal the temporally synchronised nanosecond and picosecond

laser pulses. Such facilities already exist in out country and abroad (for instance, the 'PICO' Nd laser [28] at the P.N. Lebedev Physics Institute, Russian Academy of Sciences).

Figure 1 is a schematic representation of the proposed experiment. The main nanosecond heating pulse produces the plasma plume in which SMFs are generated. The other (picosecond) beam irradiates a special target to form an electric beam. This beam propagates perpendicular to the incident first laser beam and is scattered by the SMFs. The required electron energy can be estimated. The electron scattering angle due to Coulomb collisions during passage through a plasma layer of thickness R_m is [29]

$$\langle \phi^2 \rangle = \frac{8\pi L_Q e^4 \langle N R_m \rangle}{E_e^2} = 0.31 \frac{Z}{A} \frac{\langle \rho R_m \rangle L_Q}{E_e^2 [\mathrm{MeV}]}. \quad (1)$$

Here, L_Q is the Coulomb logarithm; Z and A are the charge and atomic mass of the ions; E_e is the electron energy in MeV; ρ and N are the mass and electron plasma densities. It is evident from (1) that the rms scattering angle of electrons with an energy $E_e = 0.1$ MeV for typical plasma parameters in modern experiments on single-beam laser facilities ($\langle \rho R_m \rangle \simeq (3-5) \times 10^{-5}$ g cm^{-3}, $L_Q \sim 10$) will be less than 0.1 rad, while the Larmor radius R_L of these electrons in a 1-MGs magnetic field will be equal to ~ 10.6 μm (for a transverse plasma dimension of ~ 100 μm). Below we show on the basis of numerical calculations that the deflection angles for fast electrons with an energy of ~ 100 keV in megagauss magnetic fields will be equal to ~ 1 rad.

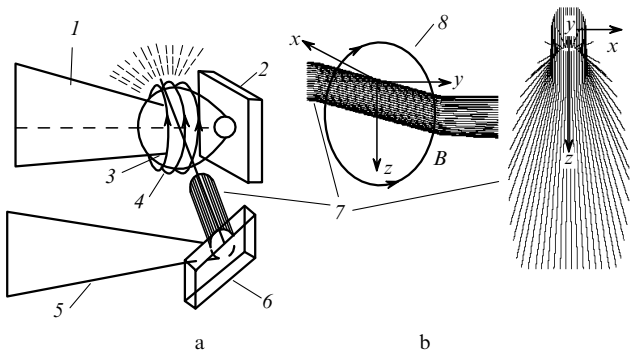

Figure 1. Schematic of the experiment to observe SMFs in a plasma plume (a) and electron trajectories in the scattering by plasma SMFs (b): (*1*) laser pulse; (*2*) target; (*3*) plasma; (*4*) magnetic field B; (*5*) picosecond laser pulse; (*6*) auxiliary target intended for electron beam generation; (*7*) electron beam; (*8*) magnetic line of force.

In our opinion, the electron-beam approach to SMF measurements under discussion offers several significant advantages over the conventional optical technique.

First, it is possible in principle to generate in a three-dimensionally nonuniform plasma not only toroidal fields, but also poloidal fields (Fig. 2). Poloidal fields are extremely difficult to observe using the traditional optical technique, because the probe beam will encounter an opaque target. When an electron beam is used, in a poloidal field it will deflect primarily in the plane perpendicular to that in which the beam deflects in the case of toroidal fields.

Second, the optical technique does not permit investigating the field in the above-critical plasma region. This limitation does not exist for the electron beam.

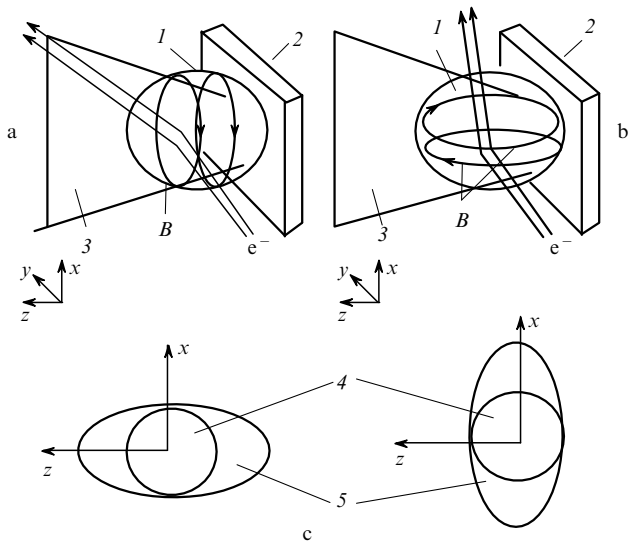

Figure 2. Schemes of electron propagation through the plasma in the case of toroidal (a) and poloidal (b) magnetic fields as well as scheme of electron distribution in the incident electron beam and the beam emerging from the plasma (c): (*1*) plasma plume; (*2*) target; (*3*) laser pulse; (*4*) electron beam entering the field; (*5*) beam scattered by the field.

Finally, the proposed technique, as mentioned above, holds promise for compressed laser targets, where the optical technique is impossible to employ. True, this will necessitate relativistic electron beams with an energy of 4–10 MeV [30]. It is noteworthy that the electron free path $l_e \sim E_e^2$, while the Larmor radius $R_L \sim 1/\sqrt{E_e}$, and by varying the electron beam energy it is therefore possible, in principle, to select the parameters such that the electrons will not undergo substantial scattering due to Coulomb collisions but will undergo the effect of fields exceeding 10 MGs.

To simulate the scattering of particles by sign-changing magnetic fields in a laser-produced plasma, we developed a three-dimensional 'AURORA' program [30]. This program was earlier employed to calculate the anisotropic distribution function of charged thermonuclear particles (protons and alpha particles) escaping from the compressed target [30]. We also resorted to this program when discussing the problem of selective extraction of multiply charged ions, long-lived isomers, and positrons from the first chamber of a thermonuclear reactor with the use of specially configured magnetic fields [31].

3. Brief description of the 'AURORA' program

The employed system of equations in Cartesian coordinates has the form:

$$\frac{dV_x}{dt} = \frac{e}{m}(V_y B_z - V_z B_y) - \frac{F_x}{m},$$

$$\frac{dV_y}{dt} = \frac{e}{m}(-V_x B_z + V_z B_x) - \frac{F_y}{m}, \quad (2)$$

$$\frac{dV_z}{dt} = \frac{e}{m}(V_x B_y - V_y B_x) - \frac{F_z}{m}.$$

Here, $\boldsymbol{V} = (V_x, V_y, V_z)$ is the electron velocity vector; $\boldsymbol{B} = (B_x, B_y, B_z)$ is the magnetic induction vector; $\boldsymbol{F} = (F_x, F_y, F_z)$ is the deceleration force; e and m are the electron charge and mass. We assume below that the Coulomb collisions and the radiative electron energy losses can be neglected and that the magnetic lines of force are 'wound' round the z axis (i.e., the fields possess a toroidal configuration and $B_z = 0$).

In the dimensionless form, Eqn (2) is of the form

$$\frac{\mathrm{d}V_x}{\mathrm{d}t} = \delta_B(V_y B_z - V_z B_y),$$

$$\frac{\mathrm{d}V_y}{\mathrm{d}t} = \delta_B(-V_x B_z + V_z B_x), \tag{3}$$

$$\frac{\mathrm{d}V_z}{\mathrm{d}t} = \delta_B(V_x B_y - V_y B_x).$$

The dimensionless parameter is $\delta_B = R_\mathrm{m}/R_\mathrm{L}$. We assume for simplicity that the plasma has the shape of a sphere of radius R_m with a width $\Delta_B = \Delta/R_\mathrm{m}$ of magnetic field localisation (Fig. 3).

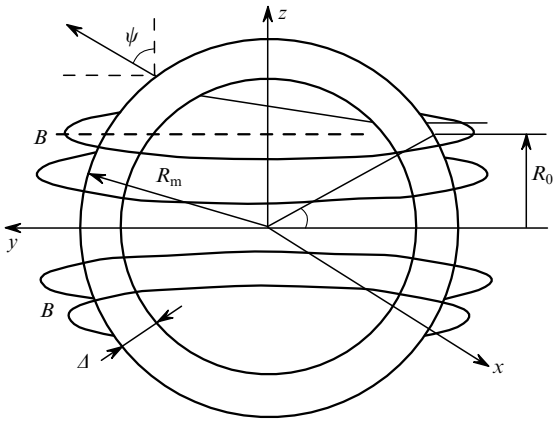

Figure 3. Schematic representation of the domain occupied by the plasma and the magnetic fields, which are localised near its boundary in a layer Δ. The electron beam travels along the y axis and has the shape of a cylinder of radius R_0. The angle ψ defines the deflection of the particle travelling direction from the initial one.

The components of magnetic field were determined from the following formulas:

$$B_x = -F(r)\sin(n\theta)\sin\varphi, \quad B_y = F(r)\sin(n\theta)\cos\varphi,$$

$$r = \left(x^2 + y^2 + z^2\right)^{1/2}, \quad \sin\varphi = \frac{y}{(x^2+y^2)^{1/2}},$$

$$\cos\varphi = \frac{x}{(x^2+y^2)^{1/2}}, \tag{4}$$

$$\theta = \begin{cases} \arctan\dfrac{(x^2+y^2)^{1/2}}{z} & \text{for } z > 0, \\ \dfrac{\pi}{2} & \text{for } z = 0, \\ \pi + \arctan\dfrac{(x^2+y^2)^{1/2}}{z}, \end{cases}$$

$$F(r) = \begin{cases} 1 & \text{for } r \in [1-\Delta_B, 1], \\ 0 & \text{for } r \notin [1-\Delta_B, 1] \end{cases} .$$

The program calculates the angles $\psi = \arcsin(V_z/V)$ and $\varphi = \arcsin(V_x/V)$ of particle deflection from the initial travelling direction as functions of the dimensionless parameters δ_B, Δ_B, and $X_0 = R_0/R_\mathrm{m}$. Because the plasma dimensions are negligible in comparison with the distance to the recording device, the dependence of the number of particles that fall into a given solid angle $[\Delta\psi, \Delta\varphi]$ on the magnitude of these angles is assumed to be the main characteristic describing the beam scattering due to SMFs.

All particles are assumed to possess the same initial velocity aligned with the y axis. The total number N_0 of the particles is uniformly 'scattered' over a circle of radius x_0 with the help of a random number generator. Subsequently, the trajectories of every particle are computed by means of the Runge–Kutta method (for more details, see Ref. [32]) and their deflection angles are calculated. The particles are 'sorted' according to their deflection angles and then the distribution function $N(\varphi, \psi)$ is constructed.

4. Main results of simulations

The results of numerical simulations are given below. We assume that the magnetic fields in the plasma plume have a purely toroidal shape, with the magnetic field harmonic $n = 1$. The patterns of the angular distribution are presented in the (φ, ψ) plane. Figure 4 shows the escape particle distribution functions for different values of the dimensionless parameter δ_B, which characterises the strength of the magnetic field. The values of parameters $\Delta_B = 0.4$ and $X_0 = 0.5$ are fixed, the number of particles is $N_0 = 5 \times 10^5$, and the number of angular intervals is 300 in all.

One can see from Fig. 4 that with increase in magnetic induction the electron deflection angles increase primarily in the yz plane, their magnitude increasing from 0.5 to 1 rad for $\delta_B \sim 1$.

For $\delta_B > 1$, a part of the particles escape from the plasma in the opposite direction, and their small fraction may find themselves captured in the magnetic trap. In particular, for $\delta_B = 5$ the fraction of reflected particles amounts to $\sim 30\,\%$ and the fraction of the captured ones is less than 1 %; for $\delta_B = 10$, up to 60 % of the particles are reflected back and only $\sim 1\,\%$ are captured in the trap. It is pertinent to note that the picture may turn out to be more complicated due to nonuniformity of the magnetic fields.

Figure 5 shows the dependences of N on the electron deflection angles φ and ψ for different parameters of the incident beam.

In the absence of the field, all particles would assemble into a point at the origin. A toroidal magnetic field displaces particles primarily in the angle ψ. The smaller the impact parameter of the beam, the more clearly defined is this displacement. But even when $X_0 \approx 1$, the prevalence of displacement in the yz plane (i.e., along the ψ axis) persists.

In the next series of calculations, we investigated the effect of the width of SMF localisation region on the electron beam scattering in relation to the parameter Δ_B (Fig. 6). As the SMF localisation region broadens, the electron scattering angles ψ increase and the picture as a whole becomes more complicated.

As base parameters we used $\delta_B = 1$, $X_0 = 0.5$, and $\Delta_B = 0.4$. When δ_B and Δ_B are significantly increased there emerge electrons which are captured by magnetic field and 'wind' round magnetic lines of force. It is clear that in real

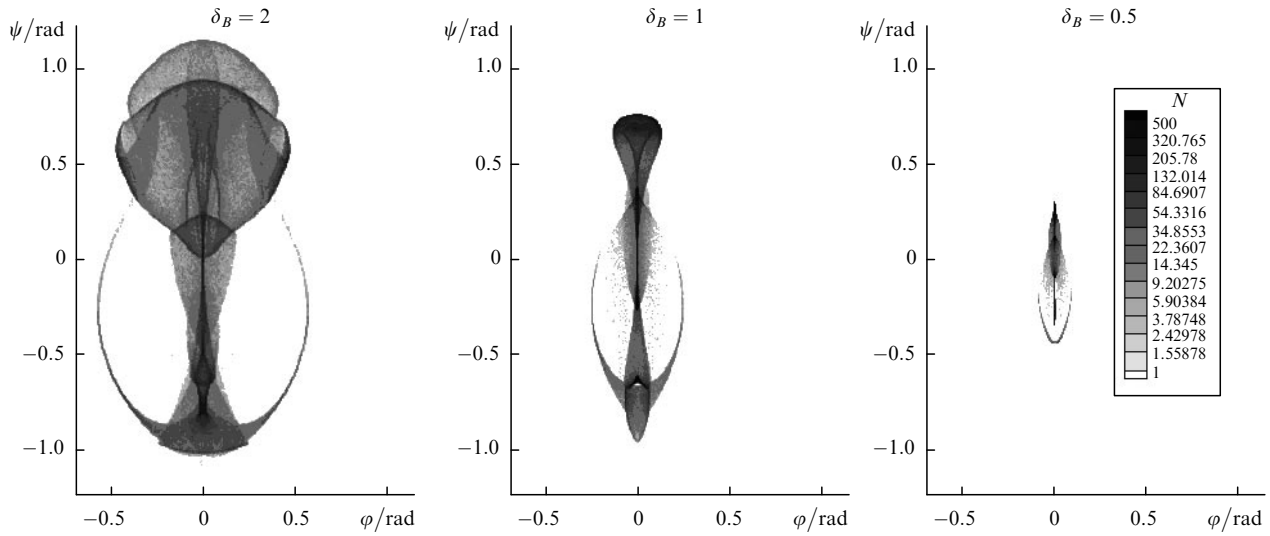

Figure 4. Dependences of the number of particles that fall into the given angular intervals $\Delta\varphi, \Delta\psi$ on the SMF strength δ_B for $\Delta_B = 0.4$ and $X_0 = 0.5$.

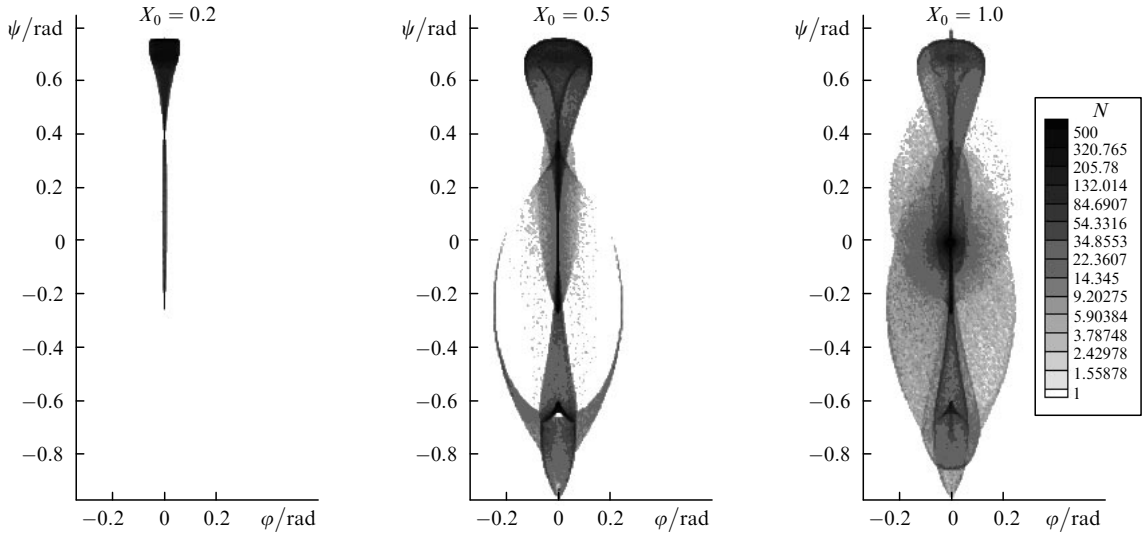

Figure 5. Dependences of the number of particles that fall into the given angular intervals $\Delta\varphi, \Delta\psi$ on the impact parameter X_0 for $\delta_B = 1$ and $\Delta_B = 0.4$.

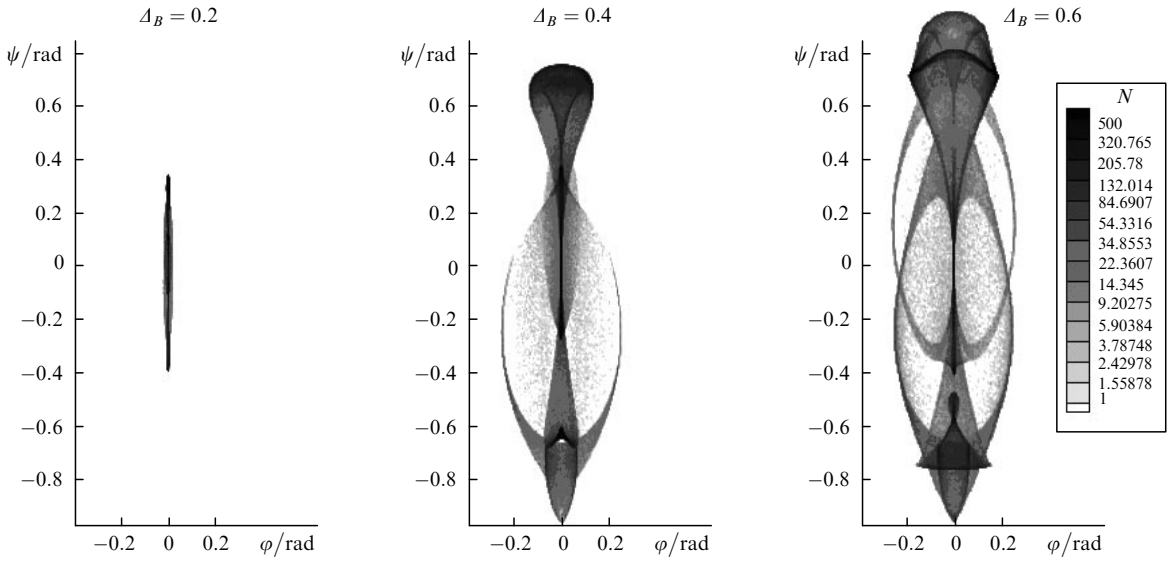

Figure 6. Effect of the width Δ_B of SMF localisation region on the electron beam scattering for $\delta_B = 1$ and $X_0 = 0.5$.

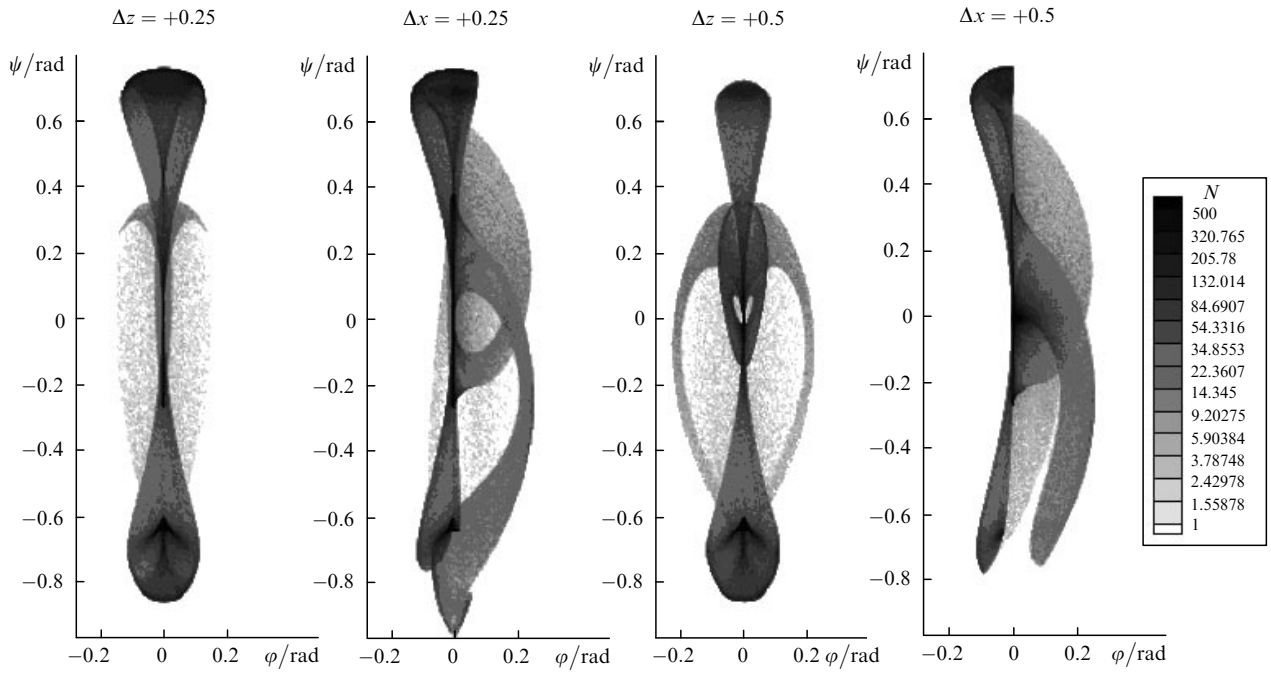

Figure 7. Effect of beam displacement along the z and x axes on the electron beam scattering for $\delta_B = 1$, $\Delta_B = 0.4$, and $X_0 = 0.5$.

situations they will escape from this 'magnetic trap' due to nonuniformity of the magnetic field and infrequent collisions. So far these effects have not been included in our simulations.

In the next series of calculations we considered the situation when the beam axis was displaced relative to the y-axis along the z and x axes by the corresponding distances Δz and Δx (Fig. 7).

When the beam axis is displaced along the z axis, the reflection image symmetry about the zero on the axis φ is preserved. This is clear, because our calculations made use of the first harmonic of magnetic field, i.e. the field direction remained invariable on displacement along the z axis. When the beam is the displaced along the x axis, the situation is different: the image symmetry about the zero on φ axis is violated, because the field above and below the zero on the x axis is different in sign.

In the case of spherical target compression, the parameter $\langle \rho R_{\rm m} \rangle$ will amount to 0.1–0.3 (in reactor-scale targets it may be much greater). To pass the electron beam through such targets requires relativistic beam energies of 4–10 MeV [30, 31]. These high-energy electrons may be obtained with the help of an additional laser providing intensities above 10^{18} W cm^{-2}. The axial symmetry in a compressed laser target is possible when the target is irradiated on both sides. For an indirect target irradiation, when the laser beams are to be converted to X-ray radiation, consideration is commonly given to laser radiation input into the converter through two openings. In these situations, SMFs will also have a toroidal topology and the harmonic numbers will be even: $n = 2, 4, \ldots, 10$.

Figure 8 shows the results of electron scattering simulations for $\delta_B = 1$, $\Delta_B = 0.4$, $X_0 = 0.5$, and $n = 2$ and 10. One can see that the beam scattering angle ψ decreases with increasing n. However, for $\delta_B = 1$ and $n \leqslant 10$, the angle $\psi > 0.1$ rad, while for the above parameters $\langle \Delta\phi^2 \rangle \leqslant 0.01$ rad^2. In this case, due to SMFs the electrons will be scattered primarily along the ψ axis, while the

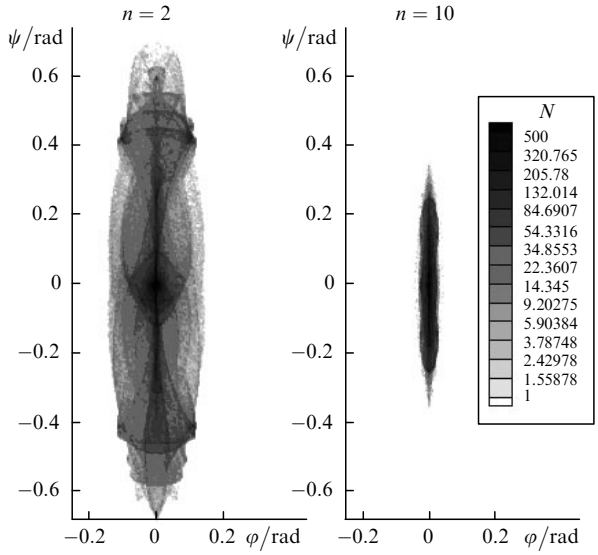

Figure 8. Dependences of the number of particles that fall into the angular intervals $\Delta\varphi$, $\Delta\psi$ on the harmonic number n for $\delta_B = 1$, $\Delta_B = 0.4$, and $X_0 = 0.5$.

collision-induced scattering in the angles φ and ψ will occur with equal probability. As indicated in the foregoing, by virtue of the corresponding energy dependences of the electron free path and the electron Larmor radius it is possible to select the beam parameters required for the observation of the effect under discussion.

In all preceding calculations the electron beam energy was assumed to be fixed. Clearly this is some idealisation of the process. In real situations, the electrons in the beam will have some velocity distribution, and extracting specifically directed electrons in a given velocity range will require sophisticated equipment. However, this is a separate question. In the context of this paper we would like to note that the existence of some spreading in electron velocities will not

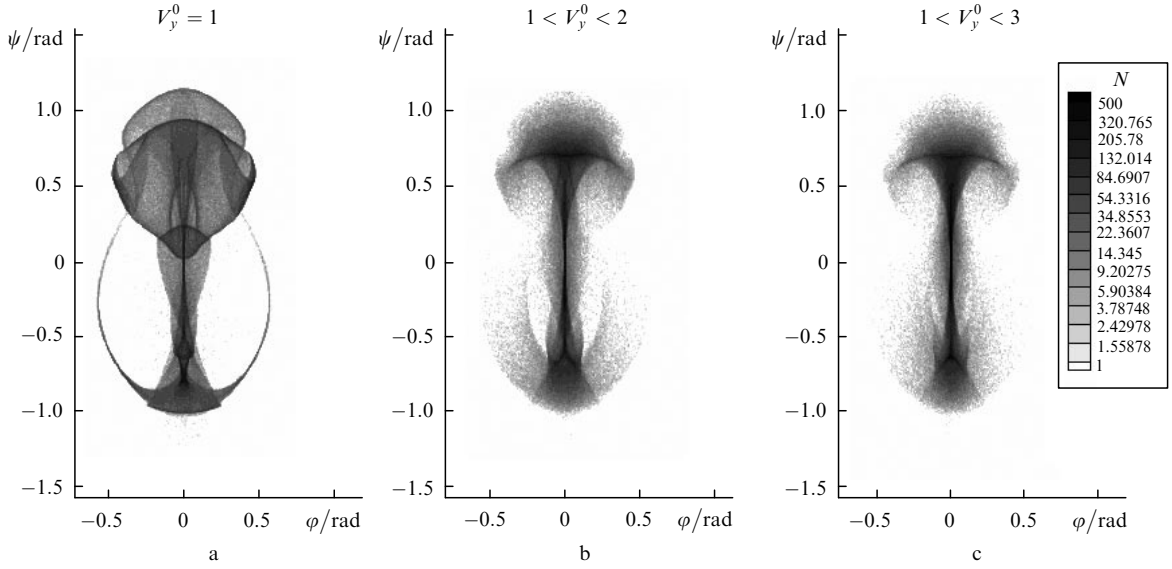

Figure 9. Dependences of the number of particles that fall into the angular intervals $\Delta\varphi, \Delta\psi$ on ΔV for $\Delta V = 0$ (a), 1 (b), and 2 (c) and $\delta_B = 1$, $\Delta_B = 0.4$, and $X_0 = 0.5$.

lead to catastrophic consequences. Figure 9 shows the results of calculations in the case when the initial particle velocities were randomly varied in the velocity range $V_y^0 = [1.1 + \Delta V]$ for different values of ΔV. The remaining parameters were fixed.

5. Conclusions

We have discussed a new approach to the investigation of SMFs in laser plasmas. The 'AURORA' program has been briefly described, and on the basis of numerical simulations we have shown that it is possible to determine the strength and localisation region dimension of these fields. It is possible to judge the SMF topology according to what plane the beam is primarily scattered in, i.e., to determine the field configuration: primarily toroidal or poloidal.

In a spherical target subject to axially symmetric irradiation, the SMFs are sign-variable. It is also possible to judge their configuration (the prevalent harmonic number) by the character of particle scattering.

References

1. Korobkin V.V., Serov R.V. *Pis'ma Zh. Eksp. Teor. Fiz.*, **4**, 103 (1966).
2. Askar'yan G.A., Rabinovich M.S., Smirnova A.D., Studenov V.B. *Pis'ma Zh. Eksp. Teor. Fiz.*, **4**, 116 (1967).
3. Stamper J.A., Papadopoulos K., Sudan R.N., et al. *Phys. Fluids*, **26**, 1012 (1971).
4. Tidman D.A., Shanny R.A. *Phys. Fluids*, **17**, 1207 (1974).
5. Bol'shov L.A., Dreizin A.M., Dykhne A.M. *Pis'ma Zh. Eksp. Teor. Fiz.*, **5**, 288 (1974).
6. Al'terkop B.A., Mishin E.V., Rukhadze A.A. *Pis'ma Zh. Eksp. Teor. Fiz.*, **5**, 291 (1974).
7. Nastoyashchii A.F. *Atomnaya Energiya*, **38**, 27 (1975).
8. Afanas'ev Yu.V., Gamalii E.G., Lebo I.G., Rozanov V.B. *Zh. Eksp. Teor. Fiz.*, **74**, 516 (1978).
9. Abdullaev A.Sh., Aliev Yu.M., Bychenkov V.Yu. *Pis'ma Zh. Eksp. Teor. Fiz.*, **28**, 524 (1978).
10. Woo W., DeGrout J.S. *Phys. Fluids*, **21**, 207 (1978).
11. Craxton R.S., Haines G. *Phys. Rev. Lett.*, **35**, 1336 (1975).
12. Colombant D.G., Winsor N.K. *Phys. Rev. Lett.*, **38**, 1336 (1977).
13. Bol'shov L.A., Dreizin Yu.A., Dykhne A.M., et al. *Zh. Eksp. Teor. Fiz.*, **77**, 2289 (1979).
14. Gamalii E.G., Gasilov V.A., Lebo I.G., et al. Preprint No. 155 (Moscow: M.V. Keldysh Institute of Applied Mathematics, USSR Academy of Sciences, 1979).
15. Stamper J.A., McLean E.A., Ripin B.H. *Phys. Rev. Lett.*, **40**, 1177 (1978).
16. Raven A., Willi O., Rumsby P.T. *Phys. Rev. Lett.*, **41**, 554 (1978).
17. Bunkin F.V., Kas'yanov Yu.S., Korobkin V.V., Motylev S.L. *Kvantovaya Elektron.*, **10**, 2149 (1983) [*Sov. J. Quantum Electron.*, **13**, 1437 (1983)].
18. Basov N.G., Wolowski E., Gamalii E.G., et. al. *Pis'ma Zh. Eksp. Teor. Fiz.*, **45**, 173 (1987) [*JETP Lett.*, **45** (4), 214 (1987)].
19. Lebo I.G. Preprint No. 64 (Moscow: P.N. Lebedev Physics Institute, USSR Academy of Sciences, 1982).
20. Gamalii E.G., Lebo I.G., Rozanov V.B. *Tr. Fiz. Inst. Akad. Nauk SSSR*, **149**, 4 (1985).
21. Kotel'nikov S.S., Lebo I.G., Rozanov V.B. *Kratk. Soobshch. Fiz.*, (1), 3 (1983).
22. Kotel'nikov S.S., Lebo I.G., Rozanov V.B. *Kratk. Soobshch. Fiz.*, (12), 58 (1986).
23. Feoktistov L.P., in *Budushchee nauki* (The Future of Science) (Moscow: Znanie, 1985) No. 18, p. 168.
24. Basov N.G., Gus'kov S.Yu., Feoktistov L.P. *J. Sov. Laser Research*, **13**, 390 (1992).
25. Tabak M., Hammer J., Glynsky M.E., Kruer W.L., et al. *Phys. Plasmas*, **1**, 1636 (1994).
26. Zvorykin V.D., Lebo I.G., Rozanov V.B. *Kratk. Soobshch. Fiz.*, (9), 20 (1997).
27. Lebo I.G. *Kvantovaya Elektron.*, **30**, 409 (2000) [*Quantum Electron.*, **30**, 409 (2000)].
28. Ivanov V.V., Knyazev A.K., Kutsenko A.V., et al. *Zh. Eksp. Teor. Fiz.*, **109**, 1257 (1996).
29. Gott Yu.V. *Vzaimodeistvie chastits s veshchestvom v plazmennykh issledovaniyakh* (Particle–Matter Interaction in Plasma Research) (Moscow: Atomizdat, 1978) p. 136.
30. Lebo I.G., Konash P.V. *Matematicheskoe Modelirovanie*, **17**, 3 (2005).
31. Lebo I.G., Konash P.V., in *54th Scientific and Technical Conf. of the Moscow State Institute of Radioengineering, Electronics, and Automation (MIREA)* (Moscow: MIREA, 2005) Part 2, p. 54.
32. Kalitkin N.N. *Chislennye metody* (Numerical Techniques) (Moscow: Nauka, 1978) p. 246.